JOURNAL OF SYNCHROTRON RADIATION

ISSN 1600-5775

Received 7 June 2021
Accepted 26 July 2021

Edited by Y. Amemiya, University of Tokyo, Japan

Keywords: microtomography; high-resolution X-ray imaging; brain imaging.

High-resolution fast-tomography brain-imaging beamline at the Taiwan Photon Source

Hsiang Hsin Chen,[a] Shun-Min Yang,[a] Kai-En Yang,[a] Ching-Yu Chiu,[a] Chia-Ju Chang,[a] Ya-Sian Wang,[a] Tsung-Tse Lee,[a] Yu-Fen Huang,[a] Yi-Yun Chen,[a] Cyril Petibois,[a] Shih-Hung Chang,[b] Xiaoqing Cai,[c] Chian-Ming Low,[d,e] Francis Chee Kuan Tan,[e] Alvin Teo,[f] Eng Soon Tok,[g] Jae-Hong Lim,[h] Jun-Ho Je,[i] Yoshiki Kohmura,[j] Tetsuya Ishikawa,[j] Giorgio Margaritondo[k,l,m] and Yeukuang Hwu[a]*

[a]Institute of Physics, Academia Sinica, 128 Academia Road Sec. 2, Taipei 11529, Taiwan, [b]National Synchrotron Radiation Research Center, Hsinchu 30076, Taiwan, [c]Shanghai Institute of Applied Physics, Chinese Academy of Science, Shanghai, People's Republic of China, [d]Department of Pharmacology, Yong Loo Lin School of Medicine, National University of Singapore, Singapore, [e]Department of Anaesthesia, National University Hospital, National University Health System, Singapore, [f]School of Chemical and Life Sciences, Nanyang Polytechnic, Singapore, [g]eMaGIC-Lab, Department of Physics, National University of Singapore, Singapore, [h]Pohang Accelerator Laboratory, Pohang University of Science and Technology, Pohang, Gyeongbuk 37673, South Korea, [i]Department of Materials Science and Engineering, Pohang University of Science and Technology, Pohang, Gyeongbuk 37673, South Korea, [j]RIKEN SPring-8 Center, Hyogo 679-5148, Japan, [k]Faculté des Sciences de Base, Ecole Polytechnique Fédérale de Lausanne, Lausanne 1015, Switzerland, [l]Brain Research Center, National Tsing Hua University, Hsinchu 30013, Taiwan, and [m]Department of Engineering Science, National Cheng Kung University, Tainan 70100, Taiwan. *Correspondence e-mail: phhwu@sinica.edu.tw

The new Brain Imaging Beamline (BIB) of the Taiwan Photon Source (TPS) has been commissioned and opened to users. The BIB and in particular its endstation are designed to take advantage of bright unmonochromatized synchrotron X-rays and target fast 3D imaging, ~1 ms exposure time plus very high ~0.3 µm spatial resolution. A critical step in achieving the planned performances was the solution to the X-ray induced damaging problems of the detection system. High-energy photons were identified as their principal cause and were solved by combining tailored filters/attenuators and a high-energy cut-off mirror. This enabled the tomography acquisition throughput to reach >1 mm^3 min^{-1}, a critical performance for large-animal brain mapping and a vital mission of the beamline.

1. Introduction

Fast 3D imaging is progressively becoming an essential technique at the Taiwan Photon Source (TPS) of the National Synchrotron Radiation Research Center, Hsinchu, Taiwan (NSRRC). Here, we present a newly commissioned beamline that supports this technique, with two critical performances: using unmonochromatized synchrotron X-rays it delivers fast image taking and high lateral resolution. We also specifically describe its new X-ray micro-imaging system that enables us to achieve such performances.

For the success of the beamline, one essential step was to limit the impact of high-energy photons from the bending magnet (BM) source spectrum. Indeed, they damage the detection system but contribute very little to the imaging contrast. By suppressing them, the beamline reaches an image-recording speed of >1 mm^3 min^{-1} and a resolution at the visible-light diffraction limit determined by the detection system.

Before the above final developments, high imaging speed and high spatial resolution were separately demonstrated

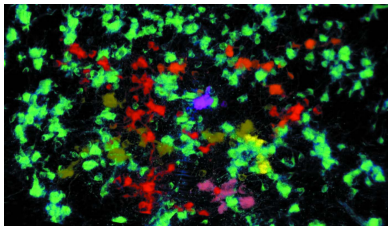

(Stampanoni *et al.*, 2006; Jung *et al.*, 2012; Zhang *et al.*, 2021; Kameshima *et al.*, 2019). However, the recently inaugurated SYNAPSE (Synchrotron for Neuroscience – an Asia–Pacific Strategic Enterprise) project (Hwu *et al.*, 2017; Chin *et al.*, 2020; https://synapse-sg.org/) requires both performances for its key objective of fully mapping the connectomes of a human brain within a few years. This required the measures described here to complete the beamline, which is part of the SYNAPSE consortium (http://www.synapse-axon.org/).

Among the facilities of SYNAPSE, the required performances were also recently achieved by the Pohang Light Source PLS-II 6c beamline, specifically capable of delivering a complete tomographic set in ∼2 min. This beamline uses a multilayer-mirror monochromator.

The solution presented here for the Brain Imaging Beamline (BIB) at TPS uses an entirely different approach to reach the required performances, with arguably more straightforward technical steps and an ample margin for further performance improvements.

We demonstrated long ago that monochromatic X-rays are not necessary to achieve high lateral resolution, nor to obtain the edge enhancement (phase contrast) for X-ray microimaging (Hwu *et al.*, 1999, 2002; Hwu & Margaritondo, 2021). Therefore, high-speed microtomography facilities can use broadband synchrotron X-rays to accelerate the imaging acquisition (Hwu *et al.*, 2001; Tsai *et al.*, 2002; Lee *et al.*, 2011; Wu *et al.*, 2021). Frame rates of >1 kHz are now routinely implemented (Fezzaa & Wang, 2008; Weon *et al.*, 2008*a*,*b*) targeting in particular dynamic phenomena.

The magnification of transmission X-ray images by an X-ray optical device – such as a Fresnel zone plate upstream of a scintillating screen – produces high-resolution levels (∼10 nm) (Wu *et al.*, 2012*a*,*b*). The nanoscale resolution, however, sacrifices the imaging speed (Chien *et al.*, 2013). In fact, most X-ray optics devices for nanoimaging, such as zone plates (Ge *et al.*, 2018) and multilayer Laue mirrors (Nazaretski *et al.*, 2017), are chromatic and use only very narrow X-ray bands.

To achieve high resolution, several facilities – including the AXON (Accelerated X-ray Observation of Neurons) instruments (Chin *et al.*, 2020) of the SYNAPSE consortium – use scintillating screens to convert the transmitted X-rays to visible-light images, captured by a 2D sensor (Hwu & Margaritondo, 2020). The resolution, however, is diffraction limited to ∼250 nm, by the visible-light optics. The throughput is also limited by the use of X-ray monochromators that decrease the flux.

2. A critical technical problem

What limits the exploitation of the total brightness and enormous (>10^{18} photons s^{-1}) flux produced by the synchrotron source? The answer is that X-rays damage the visible-light optical devices, *e.g.* objectives. Their glass material are easily tainted by X-ray exposure (Livingston & Nurnberger, 1935; Ehrt & Vogel, 1992). Fig. 1 shows an example of such effects on a stack of glass microscope slides. In the case of our new beamline, the unattenuated unmonochromatized X-rays would make the objectives black in a few seconds.

A straightforward way to protect the glass optics, adopted at several synchrotron facilities, is to reflect the visible light from the scintillator by using a mirror while the potentially damaging X-rays pass through without entering the visible-light imaging system.

However, the working distance of a high numerical aperture (NA) lens – required for high resolution – is very short, causing a problem. For example, the 0.3 µm resolution of a standard AXON system is achieved with a 40×, NA ≃ 0.95, objective whose working distance is only ∼180 µm. This is not enough to accommodate even a very thin scintillating screen, such as Lu_2SiO_5:Tb on an ∼200 µm transparent substrate (Cecilia *et al.*, 2011).

Therefore, most microtomography systems for high-resolution applications such as brain mapping (Rodrigues *et al.*, 2021) rely on filters or monochromators to attenuate the X-rays. The objective lens can thus be placed directly behind the scintillating screen without causing its immediate burnout. For example, the AXON system implemented at the TPS 2A beamline, and other SYNAPSE instruments, uses double-crystal (Si) monochromators. The typical image-taking time with 20× magnification is ∼5 s. A tomography set of 600–1200 projections thus takes >1 h. Mapping a human brain would exceed >10^6 h, or >100 years, obviously unacceptable for SYNAPSE.

The first solution to using a broader bandwidth of synchrotron X-rays was to include a high-bandpass multilayer-mirror monochromator at the 6C beamline PLS-II. The beamline thus yields a photon flux ∼20× higher than the one mentioned above (Lim *et al.*, 2017). The damage to visible-light objectives is weak enough for a few weeks of operation. It allows a fast high-resolution (<0.3 µm) tomography throughput, reaching ∼2 min with a 20× (0.75 NA) magnification. This is the present benchmark for AXON instruments of SYNAPSE.

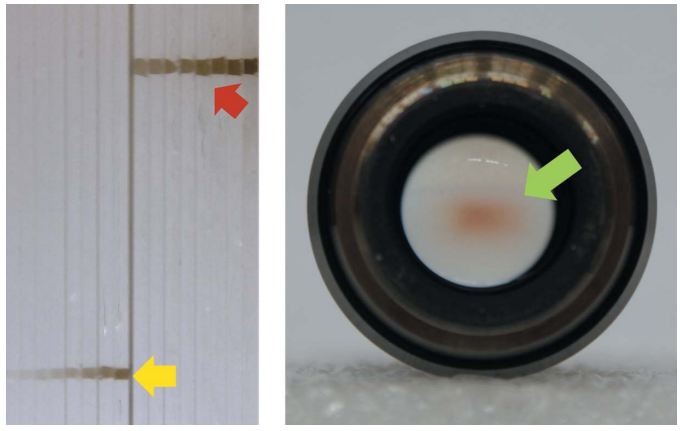

Figure 1
X-ray coloring of glass. Irradiation for 10 min with unmonochromatized BM X-rays (marked in red) and with BM X-rays filtered by an Au-coated mirror at 0.20° grazing incidence (marked in yellow) (left). Coloring of an objective lens (marked in green) after a few days of irradiation during image taking for high-speed tomography (right).

However, the bandpass of multilayer-mirror monochromators is still very narrow (André *et al.*, 2002; Mokso *et al.*, 2011; Vegso *et al.*, 2019). Therefore, we describe here an entirely different approach implemented at the BIB of TPS, based on optimizing the BM X-rays with a combination of carefully chosen filters and a high-energy cut-off total-reflection mirror. This strategy already yields resolution and throughput performances comparable with or better than multilayer monochromators, with straightforward instrumentation and the potential for significant improvements.

3. The beamline

The TPS 2A BIB receives X-rays from a BM of the 3 GeV TPS storage ring (Chang *et al.*, 2019). The BM critical energy (E_c) is 7.17 keV.

Fig. 2 shows BM spectra using data from the Center for X-ray Optics (CXRO) (Henke *et al.*, 1993; https://henke.lbl.gov/optical_constants/) within 1.2 mrad of the horizontal radiation area. A brilliance of 10^{15}–10^{16} photons s^{-1} $mrad^{-2}$ mm^{-2} (0.1% bandwidth)$^{-1}$ and a photon flux of 10^{12}–10^{13} photons s^{-1} (0.1% bandwidth)$^{-1}$ in the energy range 5–25 keV are estimated. Within this range, the horizontal and vertical source sizes are ∼92.8 µm and 38.3 µm. The horizontal source divergence is 1.2 mrad, limited by a mask aperture; the vertical source divergence varies over the spectral range, 5–25 keV, from 0.286 to 0.128 mrad. These calculations were confirmed with the *SPECTRA* (Chang *et al.*, 2019; Tanaka & Kitamura, 2001) and *SHADOW* (Lai & Cerrina, 1986; Welnak *et al.*, 1994) programs.

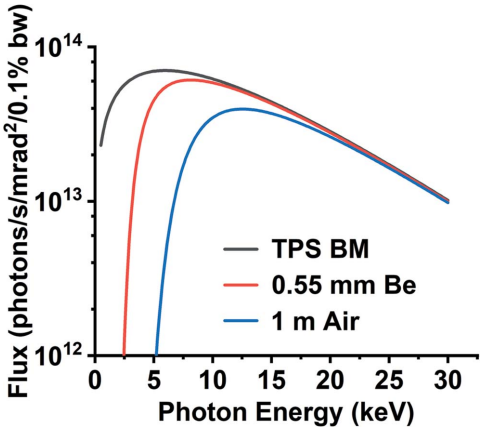

Figure 2
Calculated photon flux of a standard TPS BM line, and with 0.55 mm of Be or with 1 m of air fly pass.

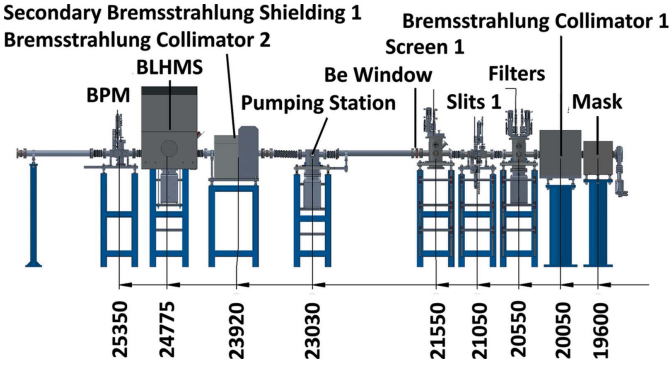

Figure 3
Layout of the TPS 02A beamline (BIB) (units in mm). BLHMS stands for the beamline heavy metal shutter.

Fig. 3 shows the layout of the beamline components, including the mask, the filters, a retractable phosphorous screen and the beam-position monitor (BPM). The monochromator, however, was not included in the configuration described in this article, which uses unmonochromatized X-rays.

4. The image station

Our solution for the problems mentioned above considers the fact that X-ray filters are high-pass devices that attenuate the unmonochromatized X-rays more efficiently on the low-energy side of the BM spectrum, which is the main contributor to the image contrast. However, high-energy X-rays are highly penetrating and cause the coloring of the glass optics. Therefore, a low-energy bandpass filter is effective in increasing the imaging throughput without damage to the optics.

Another effective approach for low-pass filtering is to use the energy-dependent total reflection. This is usually achieved with a reflective mirror at grazing incidence for the X-ray beam. Fig. 4 shows the spectrum of X-rays reflected by an Au mirror with an estimated 1 nm surface roughness. The reflectivity curve calculated by the ray-tracing software *SHADOW* and Au coating is selected for giving high critical angles for most of the photon energy of interest to the BIB, so a 300 mm-long mirror could intercept >10 mm (vertical direction) of X-ray beam to illuminate the whole field of view.

The critical angle of total reflection monotonically decreases with photon energy. One can thus select the cut-off energy and the critical angle for low-pass filtering. The typical specimens for SYNAPSE are 2–3 mm thick, thus a suitable cut-off photon energy is ∼20 keV, with the mirror tilted by ∼0.2–0.25° from the incident beam.

Fig. 4(*c*) shows the estimated total number of photons reflected by mirrors with different incident angles. Although only a small portion of the photons is filtered, the tests with glass plates demonstrate a significant coloring reduction. However, the glass coloring happened in a few minutes, requiring further attenuation.

Fig. 5(*a*) shows the X-rays passing through the combined Au mirror and thin filters. A reduction of ∼10^3–10^4 is achieved with an additional filter, and, as shown in Fig. 5(*b*), these filters also strongly suppress photons with energy higher than their characteristic absorption. A thin 250 µm Ag foil, for example, is particularly effective in attenuating above 25 keV.

Fig. 5(*c*) shows that the Au mirror and Ag attenuator combination is very effective in cutting the flux above 25 keV. The ratio of the numbers of photons above and below 25 keV is reduced from 7.3×10^{-2} (BM output) to 1.4×10^{-3} with the reflector mirror, and to 3.0×10^{-6} by adding a 250 µm Ag attenuator. The combination of the Au mirror and Ag foil

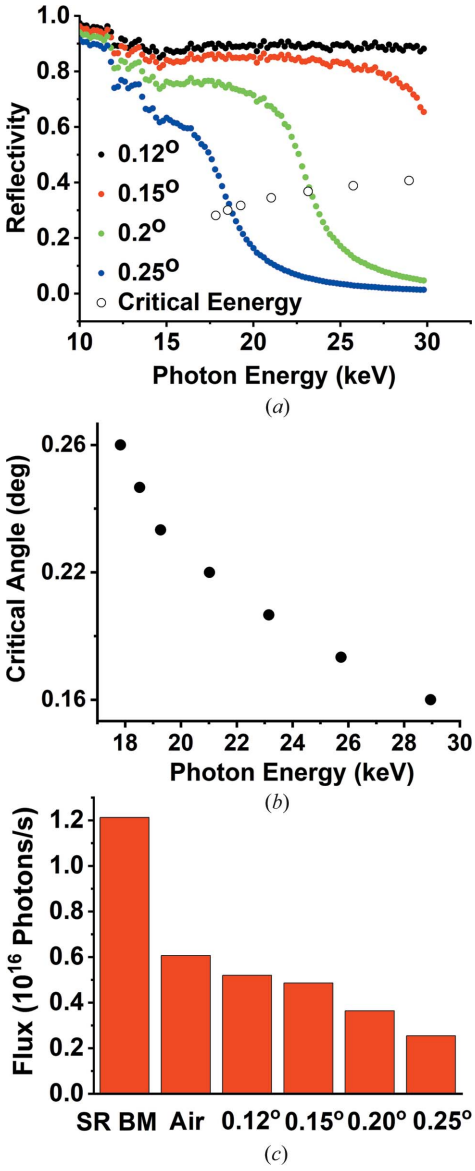

Figure 4
(*a*) Calculated X-ray reflectivity of a 300 nm Au-coated mirror as a function of the photon energy at different grazing-incidence angles. The open circles show the critical energies. (*b*) Critical angle for the Au mirror as a function of the photon energy. (*c*) Calculated total flux (0.5–30 keV) of the BIB, and with 1 m of air, and reflected by the Au-coated mirror at different incidence angles.

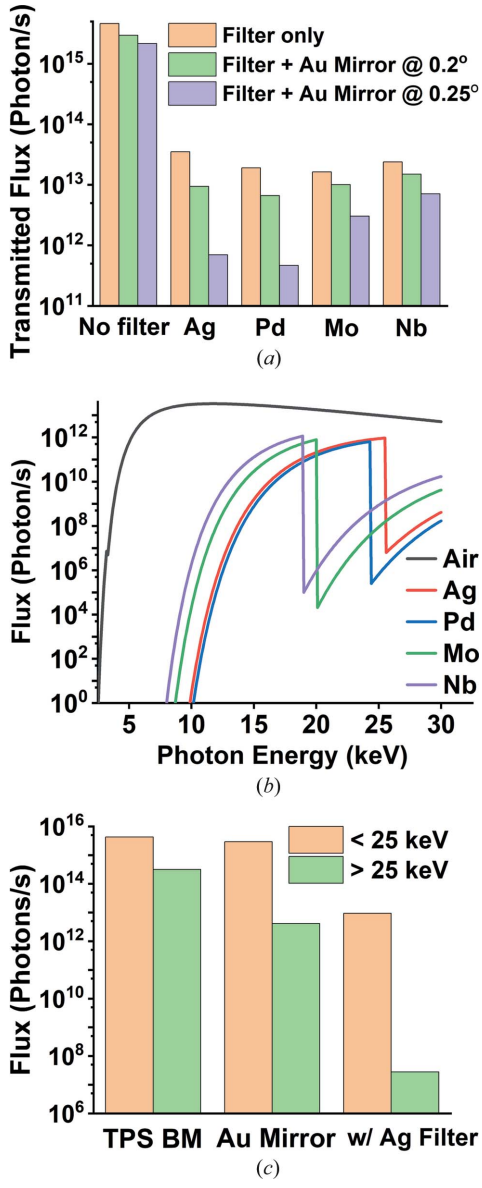

Figure 5
(*a*) Calculated photon flux transmitted through 250 µm-thick metal films and reflected by the Au-coated mirror at 0.2° and 0.25° incidence angles. (*b*) Calculated transmitted flux of 250 µm Ag, Pd, Mo and Nb foils. (*c*) Calculated total photons flux for energies above and below 25 keV, and with the Au-coated mirror at 0.25° incidence angle and with the 250 µm Ag film.

attenuates the total flux to 3×10^{-3}, a level similar to the multilayer monochromator. Tests on glass microscope slides show that the coloring is negligible.

5. The automation

The BIB operation is automated and remotely accessible as far as specimen exchange and alignment are concerned. A robotic arm is used to take each specimen, mounted on a small pedestal, from a storage plate with more than 20 samples. After imaging, the specimen is placed again in the storage plate; the entire specimen exchange can be completed in 10 s.

Good alignment is needed to guarantee that the projection images acquired during the sample rotation are suitable for accurate and reliable tomography reconstruction. This is carried out by detecting the displacement of two images taken at 180° from each other, and moving the sample rotation axis to the center of the image and perpendicular to the beam. The procedure is repeated several times if necessary.

The system can also guarantee that the image on the scintillating screen remains in the focus of the visible-light microscope. This is carried out by detecting the deterioration of the image sharpness and automatically correcting it by adjusting the microscope object position.

These automated procedures allow continuous image taking with little or no human intervention. The time they require is a reasonable 'overhead' with respect to the overall

duration of an experiment. Consider, for example, a 2 mm × 2 mm × 20 mm rod specimen. A complete experiment would include 40 1.2 mm × 1.2 mm × 1.0 mm sub-volume tomography sets, each requiring ∼2 min of image taking, for a total of 80 min. The 'overhead time' would be ∼10 min, or 11% of the total time, which is reasonable.

The tomography data are transferred in real time to the beamline computing workstations. An *ad hoc* imaging processing code processes the standard backfiltered projection images performing tomography reconstructions in the batch mode. The reconstruction takes ∼15 min for a typical tomography set of 600 2500 × 2000 pixel projection images. With the increased tomography throughput, however, new computer workstations are required to process the tomography reconstruction without backlogs.

This beamline automation decreases the overall experimental time and the required personnel. It also allows users to remotely implement experiments on their mail-in samples. This mode of operation was of course particularly important during the COVID-19 pandemic.

6. Beamline tests for ultrafast microtomography

Fig. 6 shows a reconstructed tomographic image of a mouse-brain specimen (Chin *et al.*, 2020) reaching ∼0.3 µm resolution with an Au-coated mirror and a 250 µm Ag attenuator. The time for each projection image was ∼0.1 s, giving a tomography throughput of ∼2 min, similar to that of the PLS-II 6c beamline that uses a multilayer-mirror monochromator. Fig. 7 shows the layout of the image stations with all the components described above.

7. Potential improvements

To surpass the above throughput and to fully eliminate the coloring problem, we plan a custom-made microscope objective fabricated with glass materials unaffected by X-ray coloring. The same result can also be achieved by placing a slab of a strongly X-ray absorbing optically transparent material in front of the lens, such as the $Lu_3Al_5O_{12}$ substrate of scintillating films.

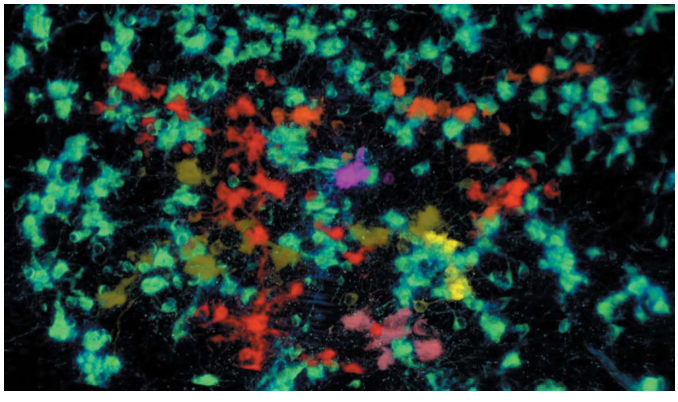

Figure 6
A 3D tomographic reconstructed image of a mouse-brain specimen. The neurons are Golgi–Cox stained and the specimen is embedded in resin (Chin *et al.*, 2020). The color coding of neurons is based on their connections: neurons of the same color are connected. The field of view is ∼750 µm.

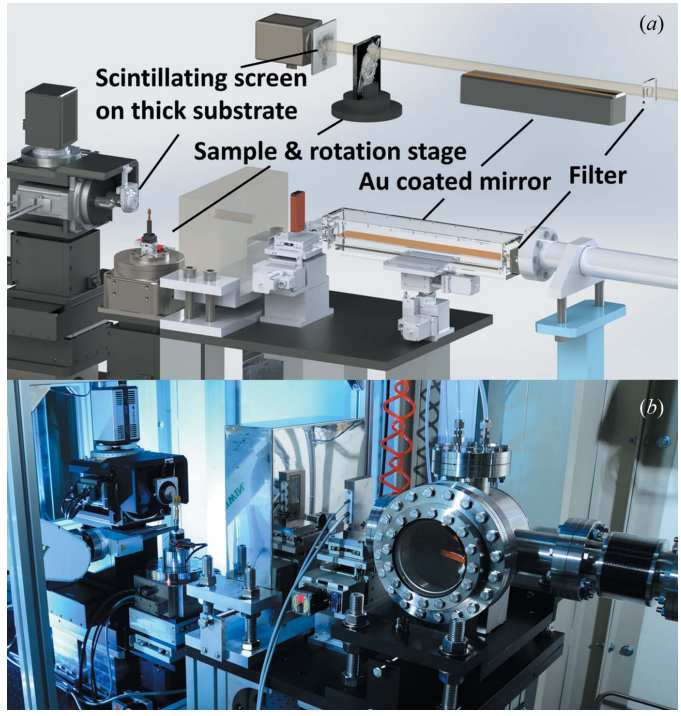

Figure 7
(*a*) Optical layout (top) and detailed 3D drawing (bottom) of the imaging system. (*b*) Photograph of the detector assembly and the sample stage.

Fig. 8 shows the X-ray attenuations of materials transparent to visible light, including LuAG ($Lu_3Al_5O_{12}$), LSO (Lu_2SiO_5) and GGG ($Gd_3Ga_5O_{12}$). Specifically, LSO would be an ideal material to protect the objectives. This would attenuate the number of photons per second reaching the objective to 3×10^{-6} (180 µm LSO) or $\sim 1 \times 10^{-12}$ (1 mm LSO). Therefore, a 1 mm-thick LSO plate will eliminate glass coloring even when using the whole BM emission and will allow us to use 10^3–10^4 more X-ray flux for tomography.

Note that the protection plate increases the objective NA as the liquid (water, oil) does for immersion lenses. Furthermore, a highly refractive substrate such as LSO or cubic ZrO_2 ($n \simeq 2.0$) can increase the NA and improve the image resolution, as confirmed by our tests on 10× and 20× lenses with a visible-light microscope.

Fig. 9 shows an X-ray micrograph of a test pattern with a transparent ∼2 mm LuAG plate behind a 180 µm-thick $CdWO_4$ scintillator taken with a 10× objective (NA = 0.45) and with a >2 mm working distance (right), and one taken without the LuAG plate (left). The addition of the LuAG plate does indeed improve the resolution. This attenuator blocks all the remaining X-rays passing through the scintillator and protects the lens from coloring.

A 250 µm Al filter, instead of an Ag filter, was used in the above test to further increase the flux. The image-recording speed was subsequently increased to ∼1 ms, an ∼10× increase

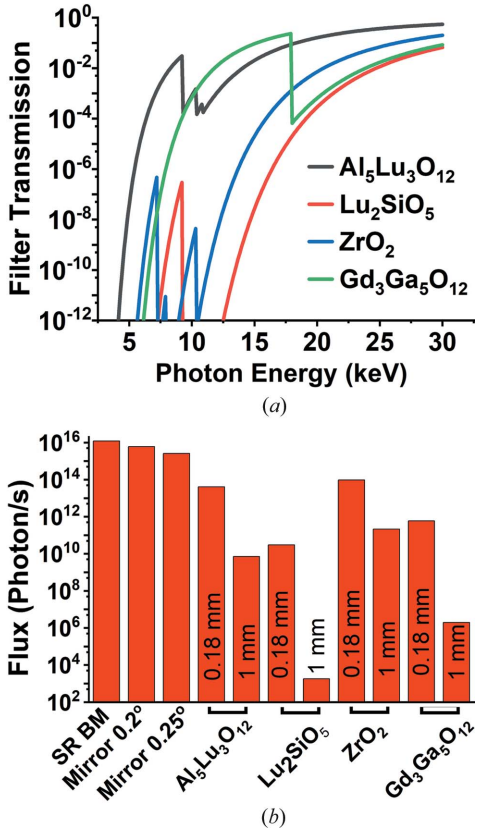

Figure 8
(*a*) X-ray transmission of 180 µm LuAG, LSO, ZrO_2 and GGG plates. (*b*) Transmitted X-ray flux of 180 µm- and 1 mm-thick LuAG, LSO, ZrO_2 and GGG materials with an Au-coated mirror at 0.25° incidence angle.

in throughput. We did not evaluate the maximum imaging speed by removing the entrance-side filter, since we expected that another 10^3 increase of flux would damage the Au coating of the reflective mirror. Our current imaging system is not optimized for fast shutter speed, <1 ms, and high image frame rate, >100 Hz (Mokso *et al.*, 2017). Moreover, the current sample rotation mechanism for tomography cannot operate at high speed to take advantage of the 1 ms exposure (Mashita *et al.*, 2021).

Using high-refractive-index materials to protect the objective lens will enable us to obtain objectives with a large field of view, 5× or 10×, and a large NA, maintaining a 0.3 µm resolution. Such improvements will be beneficial for the tomography-imaging throughput.

It is also much easier to fabricate an objective lens with sufficient working distance to incorporate a thick slab of X-ray absorbing materials than to manufacture the entire objective with materials other than glass. The development and fabrication of both types of lenses are underway.

8. Conclusions

We completed the BM BIB at TPS by implementing a new X-ray tomography imaging system, targeting optimized throughput microtomography with <0.3 µm resolution. Using a thin metal filter and a flat Au-coated mirror, we took full advantage of the BM radiation and reached the targeted resolution with an ∼1 $mm^3\,min^{-1}$ tomography speed, as required to map large animal brains within the SYNAPSE project.

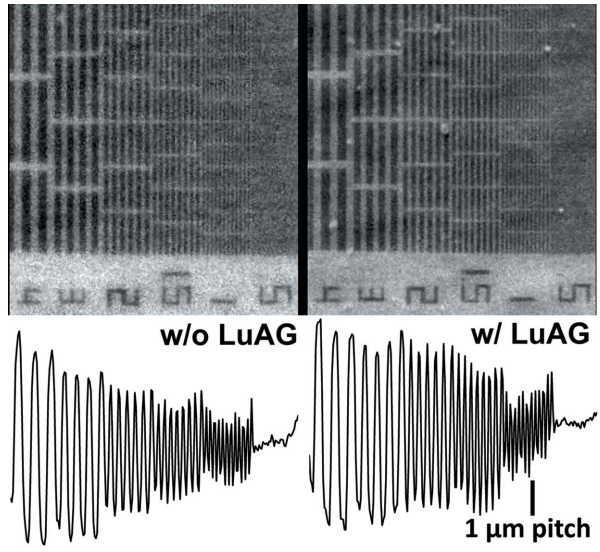

Figure 9
X-ray images of a test pattern and the corresponding line profiles taken with a 10× objective with NA ≃ 0.45. A 180 µm $CdWO_4$ scintillator with no substrate (left). A 180 µm $CdWO_4$ scintillator with 2 mm LuAG substrate (right). The resolution of the right image is better.

We proposed and preliminarily tested several improvements that will further improve the imaging time from 0.1 s to 1 ms, without degrading the 3D resolution. An effort is underway to combine the different technical solutions described here, including the high-frame-rate large-format image sensor and ultrafast rotation stage with high precision. This is in preparation for the next phase of the SYNAPSE project but it will predictably have a positive impact on other tomography applications.

Acknowledgements

We thank the NSRRC staff for their excellent professional performance in construction of the BIB.

Funding information

The following funding is acknowledged: Ministry of Science and Technology, Taiwan (grant No. 107-2119-M-001-047); National University of Singapore (grant No. R-184-000-289-133 to Chian-Ming Low, Eng Soon Tok; grant No. R-184-000-261-101 to Chian-Ming Low; grant No. R-184-000-310-733 to Chian-Ming Low, Eng Soon Tok); National University of Singapore – National Supercomputing Center (grant No. N-184-000-042-001 to SYNAPSE Project).

References

André, J. M., Benbalagh, R., Barchewitz, R., Ravet, M. F., Raynal, A., Delmotte, F., Bridou, F., Julié, G., Bosseboeuf, A., Laval, R., Soullié, G., Rémond, C. & Fialin, M. (2002). *Appl. Opt.* **41**, 239–244.

Cecilia, A., Rack, A., Douissard, P.-A., Martin, T., dos Santos Rolo, T., Vagovič, P., Pelliccia, D., Couchaud, M., Dupré, K. & Baumbach, T. (2011). *Nucl. Instrum. Methods Phys. Res. A*, **633**, S292–S293.
Chang, S.-H., Chang, C. Y., Liu, C. Y., Chang, C. F., Chiang, L. C., Liao, B. Y., Chen, Y. S., Chen, H. H., Yang, S. M., Lee, T. T., Chen, Y. J., Chen, F. L. & Hwu, Y. K. (2019). *AIP Conf. Proc.* **2054**, 060042.
Chien, C. C., Tseng, P. Y., Chen, H. H., Hua, T. E., Chen, S. T., Chen, Y. Y., Leng, W. H., Wang, C. H., Hwu, Y., Yin, G. C., Liang, K. S., Chen, F. R., Chu, Y. S., Yeh, H. I., Yang, C. S., Yang, C. S., Zhang, G. L., Je, J. H. & Margaritondo, G. (2013). *Biotechnol. Adv.* **31**, 375–386.
Chin, A. L., Yang, S. M., Chen, H. H., Li, M. T., Lee, T. T., Chen, Y. J., Lee, T. K., Petibois, C., Cai, X., Low, C. M., Tan, F. C. K., Teo, A., Tok, E. S., Ong, E. B. L., Lin, Y. Y., Lin, I. J., Tseng, Y. C., Chen, N. Y., Shih, C. T., Lim, J. H., Lim, J., Je, J. H., Kohmura, Y., Ishikawa, T., Margaritondo, G., Chiang, A. S. & Hwu, Y. (2020). *Chin. J. Phys.* **65**, 24–32.
Ehrt, D. & Vogel, W. (1992). *Nucl. Instrum. Methods Phys. Res. B*, **65**, 1–8.
Fezzaa, K. & Wang, Y. (2008). *Phys. Rev. Lett.* **100**, 104501.
Ge, M., Coburn, D. S., Nazaretski, E., Xu, W., Gofron, K., Xu, H., Yin, Z. & Lee, W. K. (2018). *Appl. Phys. Lett.* **113**, 083109.
Henke, B. L., Gullikson, E. M. & Davis, J. C. (1993). *At. Data Nucl. Data Tables*, **54**, 181–342.
Hwu, Y., Lai, B., Mancini, D. C., Je, J. H., Noh, D. Y., Bertolo, M., Tromba, G. & Margaritondo, G. (1999). *Appl. Phys. Lett.* **75**, 2377–2379.
Hwu, Y. & Margaritondo, G. (2020). *IEEE Sens. J.* **21**, 12764–12773.
Hwu, Y. & Margaritondo, G. (2021). *J. Synchrotron Rad.* **28**, 1014–1029.
Hwu, Y., Margaritondo, G. & Chiang, A. S. (2017). *BMC Biol.* **15**, 122.
Hwu, Y., Tsai, W. L., Groso, A., Margaritondo, G. & Je, J. H. (2002). *J. Phys. D Appl. Phys.* **35**, R105–R120.
Hwu, Y., Tsai, W. L., Hsieh, H. H., Ho Je, J., Kang, H. S., Kim, I. W., Lee, K. H., Kim, H. J., Lai, B. & Margaritondo, G. (2001). *Nucl. Instrum. Methods Phys. Res. A*, **467–468**, 1294–1300.
Jung, J. W., Lee, J. S., Kwon, N., Park, S. J., Chang, S., Kim, J., Pyo, J., Kohmura, Y., Nishino, Y., Yamamoto, M., Ishikawa, T. & Je, J. H. (2012). *Rev. Sci. Instrum.* **83**, 093704.
Kameshima, T., Takeuchi, A., Uesugi, K., Kudo, T., Kohmura, Y., Tamasaku, K., Muramatsu, K., Yanagitani, T., Yabashi, M. & Hatsui, T. (2019). *Opt. Lett.* **44**, 1403–1406.
Lai, B. & Cerrina, F. (1986). *Nucl. Instrum. Methods Phys. Res. A*, **246**, 337–341.
Lee, J. S., Weon, B. M., Park, S. J., Je, J. H., Fezzaa, K. & Lee, W. K. (2011). *Nat. Commun.* **2**, 367.
Lim, J.-H., Seo, S.-J., Kim, H.-Y., Ryu, C. K., Rah, S., Huang, J. Y., Lee, C.-S., Seo, I. D., Kim, S.-G., Lee, D. & Cho, M.-H. (2017). *Biodesign*, **5**, 53–61.
Livingston, R. & Nurnberger, C. E. (1935). *J. Phys. Chem.* **39**, 1011–1020.
Mashita, R., Yashiro, W., Kaneko, D., Bito, Y. & Kishimoto, H. (2021). *J. Synchrotron Rad.* **28**, 322–326.
Mokso, R., Marone, F., Haberthür, D., Schittny, J. C., Mikuljan, G., Isenegger, A., Stampanoni, M., McNulty, I., Eyberger, C. & Lai, B. (2011). *AIP Conf. Proc.* **1365**, 38–41.
Mokso, R., Schlepütz, C. M., Theidel, G., Billich, H., Schmid, E., Celcer, T., Mikuljan, G., Sala, L., Marone, F., Schlumpf, N. & Stampanoni, M. (2017). *J. Synchrotron Rad.* **24**, 1250–1259.
Nazaretski, E., Yan, H., Lauer, K., Bouet, N., Huang, X., Xu, W., Zhou, J., Shu, D., Hwu, Y. & Chu, Y. S. (2017). *J. Synchrotron Rad.* **24**, 1113–1119.
Rodrigues, P. V., Tostes, K., Bosque, B. P., de Godoy, J. V. P., Amorim Neto, D. P., Dias, C. S. B. & Fonseca, M. C. (2021). *Front. Neurosci.* **15**, 627994.
Stampanoni, M., Groso, A., Isenegger, A., Mikuljan, G., Chen, Q., Bertrand, A., Henein, S., Betemps, R., Frommherz, U., Bohler, P., Meister, D., Lange, M. & Abela, R. (2006). *Proc. SPIE*, **6318**, U199–U212.
Tanaka, T. & Kitamura, H. (2001). *J. Synchrotron Rad.* **8**, 1221–1228.
Tsai, W. L., Hsu, P. C., Hwu, Y., Chen, C. H., Chang, L. W., Je, J. H., Lin, H. M., Groso, A. & Margaritondo, G. (2002). *Nature*, **417**, 139.
Vegso, K., Wu, Y., Takano, H., Hoshino, M. & Momose, A. (2019). *Sci. Rep.* **9**, 7404.
Welnak, C., Chen, G. C. & Cerrina, F. (1994). *Nucl. Instrum. Methods Phys. Res. A*, **347**, 344–347.
Weon, B. M., Je, J. H., Hwu, Y. & Margaritondo, G. (2008*a*). *Phys. Rev. Lett.* **100**, 217403.
Weon, B. M., Je, J. H., Hwu, Y. & Margaritondo, G. (2008*b*). *J. Synchrotron Rad.* **15**, 660–662.
Wu, H. R., Chen, S. T., Chu, Y. S., Conley, R., Bouet, N., Chien, C. C., Chen, H. H., Lin, C. H., Tung, H. T., Chen, Y. S., Margaritondo, G., Je, J. H. & Hwu, Y. (2012*a*). *J. Phys. D Appl. Phys.* **45**, 242001.
Wu, S.-R., Hwu, Y. & Margaritondo, G. (2012*b*). *Materials*, **5**, 1752–1773.
Wu, Y., Takano, H. & Momose, A. (2021). *Rev. Sci. Instrum.* **92**, 043702.
Zhang, Z., Wang, C., Koe, B., Schlepütz, C. M., Irvine, S. & Mi, J. (2021). *Acta Mater.* **209**, 116796.